Refined crystal structure of DsRed, a red fluorescent protein from coral, at 2.0-Å resolution

Daniel Yarbrough*, Rebekka M. Wachter*, Karen Kallio*, Mikhail V. Matz†‡, and S. James Remington*§

*Departments of Physics and Biology and the Institute of Molecular Biology, University of Oregon, Eugene, OR 97403; and †Institute for Bioorganic Chemistry, Russian Academy of Science, 117871 Moscow, Russia

Communicated by Brian W. Matthews, University of Oregon, Eugene, OR, November 8, 2000 (received for review October 5, 2000)

The crystal structure of DsRed, a red fluorescent protein from a corallimorpharian, has been determined at 2.0-Å resolution by multiple-wavelength anomalous dispersion and crystallographic refinement. Crystals of the selenomethionine-substituted protein have space group $P2_1$ and contain a tetramer with 222 noncrystallographic symmetry in the asymmetric unit. The refined model has satisfactory stereochemistry and a final crystallographic *R* factor of 0.162. The protein, which forms an obligatory tetramer in solution and in the crystal, is a squat rectangular prism comprising four protomers whose fold is extremely similar to that of the *Aequorea victoria* green fluorescent protein despite low (≈23%) amino acid sequence homology. The monomer consists of an 11-stranded β barrel with a coaxial helix. The chromophores, formed from the primary sequence -Gln-Tyr-Gly- (residues 66–68), are arranged in a ≈27 × 34-Å rectangular array in two approximately antiparallel pairs. The geometry at the α carbon of Gln-66 (refined without stereochemical restraints) is consistent with an sp^2 hybridized center, in accord with the proposal that red fluorescence is because of an additional oxidation step that forms an acylimine extension to the chromophore [Gross, L. A., Baird, G. S., Hoffman, R. C., Baldridge, K. K. & Tsien, R. Y. (2000) *Proc. Natl. Acad. Sci. USA* 87, 11990–11995]. The carbonyl oxygen of Phe-65 is almost 90° out of the plane of the chromophore, consistent with theoretical calculations suggesting that this is the minimum energy conformation of this moiety despite the conjugation of this group with the rest of the chromophore.

DsRed, a bright red fluorescent protein recently cloned from a corallimorpharian of the *Discosoma* genus, has considerable potential to complement existing uses of the extremely popular *Aequorea victoria* green fluorescent protein (avGFP) (for reviews, see refs. 1 and 2). Several fluorescent proteins (FPs) homologous to avGFP have been discovered in *Anthozoa* representatives. They function in part to contribute to the natural coloration of their hosts, and/or possibly as one means of protection against UV radiation (3–5). Of particular interest are red-emitting ($\lambda_{max} > 580$ nm) FPs. In addition to their use in multicolor tagging experiments, these could, in principle, be very helpful by avoiding natural cellular autofluorescence and by extending the range of resonance energy transfer-based experiments (1). In this application, fluorescence resonance energy transfer between pairs of FPs may find use in the detection of protein–protein interactions or other proximity-related phenomena *in vivo*. One such red-emitting FP is commercially available from CLONTECH under the trade name of DsRed.

DsRed, a 28-kDa polypeptide, has essentially the same chromophore as avGFP, autocatalytically formed from an internal Gln-Tyr-Gly (residues 66–68) tripeptide (amino acid sequence numbering of wild-type protein) (4). The overall amino acid sequence homology to avGFP is low, about 23%; however, several amino acids in the immediate vicinity of the chromophore are strictly conserved and are probably essential for chromophore formation (e.g., Glu-215 and Arg-95, corresponding to avGFP Glu-222 and Arg-96). The broad excitation and emission bands have maxima at 558 and 583 nm, respectively (with a minor peak at 494 nm and a significant tryptophan peak at 280 nm) for a monomer extinction coefficient and fluorescence quantum yield at 558 nm of approximately 75,000 mol^{-1}/cm^{-1} and 0.7, respectively (6). DsRed is an excellent fluorescence resonance energy transfer counterpart to the yellow fluorescent variants of avGFP, which have emission maxima of about 525 nm (7, 8), and its emission is distinct from that of avGFP for double-labeling experiments.

DsRed takes days to mature at room temperature and apparently passes through an obligatory green-emitting intermediate (6, 9) similar to avGFP. Point mutants have been found (e.g., K83R, K70M) that prevent the protein from maturing beyond the green stage, and another (K83M) substantially redshifts the emission from the normal maximum of 583 nm to 602 nm. Maturation requires molecular oxygen, and there is evidence that formation of the red-emitting chromophore does not go beyond 50% completion (10). Gross *et al.* (10) have proposed that the final step of maturation involves oxidation of the bond between the α carbon and the nitrogen of Gln-66 to form an acylimine, which extends the conjugation of the chromophore, as diagrammed in Scheme 1.

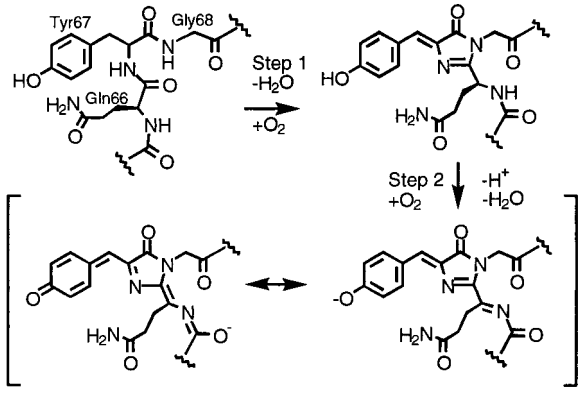

Scheme 1.

Finally, the mature protein has been shown by analytical ultracentrifugation to form an obligate tetramer in solution (6) and may form higher-order oligomers under certain conditions.

Several properties of DsRed are both puzzling and undesirable for a genetic marker. The slow maturation, apparent incomplete chromophore formation, and obligate oligomerization will lead to

Abbreviations: FPs, fluorescent proteins; avGFPs, *Aequorea victoria* green FPs.

Data deposition: The atomic coordinates and structure factors have been deposited in the Protein Data Bank, www.rcsb.org (PDB ID codes 1G7K, R1G7KSF).

‡Present address: Whitney Laboratory, University of Florida, 9505 Ocean Shore Boulevard, St. Augustine, FL 32086.

§To whom reprint requests should be addressed at: Institute of Molecular Biology, University of Oregon, Eugene, OR 97403. E-mail: jim@uoxray.uoregon.edu.

The publication costs of this article were defrayed in part by page charge payment. This article must therefore be hereby marked "*advertisement*" in accordance with 18 U.S.C. §1734 solely to indicate this fact.

problems as a marker for gene expression or protein localization *in vivo*. Tetramer formation is especially problematic as a result of the unwanted association of proteins to which DsRed is covalently linked, for example, membrane proteins. Knowledge of the three-dimensional structure would clearly be advantageous in alleviating these problems, but a structural basis for the understanding of the fundamental photophysics and maturation chemistry is desirable in its own right. To provide one basis for further investigation into the properties of DsRed, we have used multiwavelength anomalous dispersion and crystallographic refinement to define the structure of the molecule at 2.0-Å resolution.

Materials and Methods

DsRed was expressed in *Escherichia coli* (JM-109) by use of the pQE-30 expression system with an amino-terminal His6 tag (kindly provided by CLONTECH), with selenomethionine incorporation as described (11). Protein was purified by Ni^{2+} affinity chromatography over Ni-NTA agarose (Qiagen, Chatsworth, CA), dialyzed against 300 mM NaCl, 50 mM Hepes (pH 7.9), and then buffer exchanged with PD-10 Sephadex columns (Amersham Pharmacia) into 2 mM β-mercaptoethanol, 300 mM NaCl, 20 mM Tris (pH 7.9) (salt was necessary for protein solubility at high concentration). Samples were concentrated to ≈15 mg/ml by filtration (Centricon 10; Amicon). Crystals were grown in 1–2 weeks by hanging drop vapor diffusion against 16% polyethylene glycol 1550, 0.1 M Tris (pH 7.4), with 1 μl β-mercaptoethanol per well. Drops were 3 μl of protein solution and 3 μl of well solution, and microseeding was carried out 24 h after wells were set up. For low-temperature diffraction data collection, crystals were then exchanged over 8 h into a solution of 20% polyethylene glycol 1550, 20% ethylene glycol, 0.1 M Tris (pH 7.5), and 5 mM β-mercaptoethanol.

Diffraction data were collected from a single frozen crystal at three wavelengths for multiwavelength anomalous dispersion phasing at beamline 9-2 at the Stanford Synchrotron Radiation Laboratory. Phasing was carried out by using SOLVE (12) to identify 22 selenium sites, parameters for which were refined by SHARP (13). The resulting electron density map was solvent flattened by using SOLOMON (14) and is of excellent quality.

The map revealed clear density for four protomers, so a model for one was constructed by using O (15), and the positions and orientations of the remaining monomers were determined by a six-dimensional real space search, fitting the α-carbon skeleton to the electron density map with the use of RSS (S.J.R., unpublished observations). Given the high quality of the map, we felt that averaging over the subunits would be unlikely to result in substantial improvement and might actually obscure some interesting features. Refinement of the model was carried out with TNT (16) without application of noncrystallographic symmetric restraints. Finally, solvent molecules were placed where evidenced by large positive difference electron density features suitably close to hydrogen bond partners.

Results and Discussion

Structure Determination. Crystals of DsRed have space group $P2_1$ with cell parameters of $a = 53.4$, $b = 112.3$, $c = 70.7$ Å, and $\beta = 93.8°$. Polar angle self-rotation function calculations with GLRF (17) were performed with 25-4 Å native data, and the $\kappa = 180°$ section revealed peaks at 7.7, 7.1, and 6.7 σ above the mean consistent with 222 local symmetry. Therefore, the asymmetric unit of the crystal contains a tetramer with 222 noncrystallographic symmetry with a packing parameter $V_m = 1.9$ Å^3/Da (18). One local axis is tipped about 12° away from *Z* in the *YZ* plane, and the other two roughly bisect the *XY* plane as defined in GLRF.

Molecular replacement procedures by using available models for avGFP failed to produce useful solutions. Therefore, we proceeded by building a preliminary model for the A monomer into the experimental electron density map and then fitting this model to the other three positions by use of a brute-force real-space search procedure, in which the search function consisted of the summed electron density at the map grid points closest to the α-carbon positions. The search was initiated by positioning the model at the approximate centers of mass of the remaining monomers by visual inspection of the electron density map. An automated search on three angles at 5° increments and a limited translation of ±5 Å (1-Å increments) about the starting position resulted in peak heights of 21, 18, and 6.4 standard deviations above the mean of the search function for monomers B, C, and D, respectively. After manual and automated crystallographic refinement, the final model statistics are as presented in Table 1. The overall stereochemistry is acceptable, and the final *R* factor is 0.162. Deviations from perfect noncrystallographic 222 symmetry of the α-carbon positions are insignificant, with r.m.s. deviations of about 0.25 Å, which is not surprising for a protein with such a rigid fold.

Overall Fold. Despite the very low level of overall amino acid sequence identity, the overall fold of DsRed is virtually identical to that of avGFP, consisting of a slightly irregular 11-stranded β-barrel [described as a "β can"(19)] with a coaxial central helix and α-helical caps on the barrel ends. A least-squares procedure was used to superimpose the backbone of monomer A of DsRed on that of monomeric avGFP [PDB code 1EMA (7)] by the procedure of Rossmann and Argos (20). By using this method (W. S. Bennett, unpublished program) with E1 = E2 = 1.0 Å, 164 α carbons superimpose to ≈1.0 Å rms. For a stereo view of this superposition, see Fig. 1.

As predicted from sequence comparisons (4), several of the loops between β strands are truncated in DsRed relative to avGFP. For the most part, this results in only minor structural changes, as can be seen in the overlay of the two models (Fig. 1). However, the loop comprising residues 201–209 is shortened markedly relative to avGFP, which has a large loop composed primarily of charged and polar residues extending far from the body of the protein, whereas DsRed has a more compact hydrophobic loop, three residues shorter, which packs tightly against the protein core. Contributing to the more compact conformation of this loop is the absence of an equivalent to Pro-211, which in avGFP helps force the loop into an extended conformation. Finally, the loop comprising residues 183–189 of DsRed is shortened considerably relative to avGFP.

Some irregularities in these highly symmetric protein structures are conserved. As in avGFP, there is a pronounced bulge in the region of the seventh β strand centered on residue DsRed Ser-146. The corresponding side-chain avGFP His-148 occupies the space between strands and partially satisfies the backbone hydrogen bonding potential in this region; however, this side chain is not required for bulge formation (8). In DsRed, the bulge is less pronounced, and strands 7 and 8 form reasonable hydrogen bonds on either side of residues 145–148. The reestablishment of hydrogen bonding on the carboxyl-terminal side of residue 148 moves the end of strand 7 closer to strand 8 and away from strand 10, opening a dramatic cleft in the surface of the molecule (Fig. 1, *Top Center*), which is present but not as pronounced in avGFP. In both cases, the carbonyl oxygens of residues avGFP146 and DsRed144 are turned inward toward the chromophore cavity in virtually identical conformations. Finally, a classic β bulge (residues 202 and 203) helps form one side of this cleft.

A number of concerted changes in the structure force main-chain residues ≈197–220 (e.g., Glu-215) and ≈140–145 much closer to the chromophore, which has direct and probably very important consequences on the chromophore environment because of side-chain placement (see below).

The Tetramer Interface. The most striking feature of DsRed is that, as shown in Fig. 2, it exists as an extremely close-packed tetramer, quite unlike the primarily monomeric avGFP. The tetramer is a squat square prism with remarkably flat sides and

Table 1. Crystallographic statistics

	Inflection wavelength, 0.97887 Å	Peak wavelength, 0.97868 Å	Remote wavelength, 0.95373 Å
Data collection			
Total observations	232,348	236,425	230,842
Unique reflections	56,118	56,164	56,056
Resolution, Å	25.1–2.00	25.1–2.00	24.1–2.00
Highest resolution shell, Å	2.11–2.00	2.11–2.00	2.10–2.00
Completeness	94.9 (95.2)	95.2 (95.5)	94.8 (95.1)
R_{merge}	0.027 (0.044)	0.029 (0.044)	0.026 (0.043)
Phasing*			
Isomorphous phasing power	9.17	8.28	3.51
Anomalous phasing power	3.76	4.26	3.51
Overall figure of merit	0.844		
Refinement			
Resolution, Å	25.1–2.0		
Number of protein atoms	7,164		
Number of solvent atoms	418		
R_{factor}[†]/R_{free}	16.2/24.9		
rms deviations			
Bond lengths, Å	0.014		
Bond angles, °	1.86		
B factor correlations, Å^2	4.1		

Values in parentheses indicate the statistics for the highest-resolution shell.
*These statistics are based on 22 selenium sites refined by SHARP.
[†]$R = \Sigma||F_{obs}|-|F_{calc}||/\Sigma|F_o|$. In the deposited coordinates, all reflections were used in refinement, $R = 0.167$.

a small elliptical hole directly through the center. The hole is lined with polar residues and salt bridges and localizes a number of solvent molecules.

The monomers are arranged as a dimer of dimers, with the A and C chains making close contacts via their surfaces and carboxy termini, and the A and B chains interact via large buried patches. The accessible surface area of the isolated monomer (21) is ≈10,230 Å^2, and that of the tetramer is 31,420 Å^2, so roughly 25% of the monomer surface is not solvent accessible in the tetramer. The two interfaces bury ≈2,400 Å^2 of surface area per monomer, distributed approximately as 1,040 Å^2 at the AB interface and 1,360 Å^2 at the AC interface.

The AB interface does not seem to have particularly notable features and consists of hydrophobic interactions between small side chains, although a few hydrogen bonds and salt bridges are also present. The sequence Val-104, Thr-106, and Thr-108, in which Thr-A106 is hydrogen bonded to its counterpart Thr-B106 (likewise for CD), is central to this interface. On the other hand, interactions in the AC (and BD) interface consist largely of salt bridges and hydrogen bonds, many of which are mediated by buried water molecules, as well a surprisingly large number of interactions involving aromatic residues. The major players at this contact are Arg-153, His-162, His-172, Leu-174, Tyr-192, Tyr-194, Arg-216, and residues 222–225. There are several interesting and unusual features in the AC and BD interfaces. A unique feature of the DsRed tetramer is the carboxy termini, which in avGFP are flexible [only residues 2–229 are visible of the 238 in the mature protein (7)]. In DsRed, the carboxy terminus of the A monomer embraces the C monomer and vice versa, forming a "clasp" about a local 2-fold. This includes the placement of His-222 and Phe-224 in pockets on the adjacent subunit, with Phe-A224 tucked into a slot between residues Arg-C216 and Glu-C218, and His-A222 is lodged between residues Ser-C146 (hydrogen bonded to the C146 carbonyl) and Asp-C196. Although the carboxyl-terminal carboxylates are par-

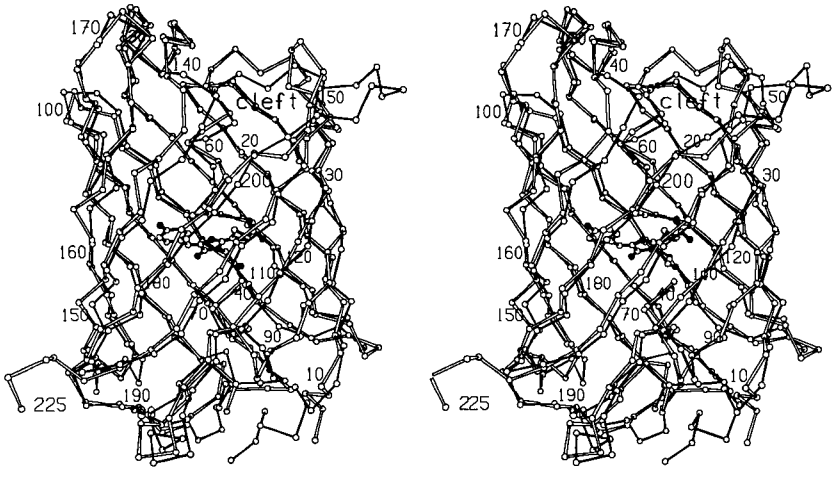

Fig. 1. Stereo view of superposition of the α-carbon backbones of avGFP (filled bonds) and DsRed (open bonds), showing the DsRed chromophore in ball-and-stick representation.

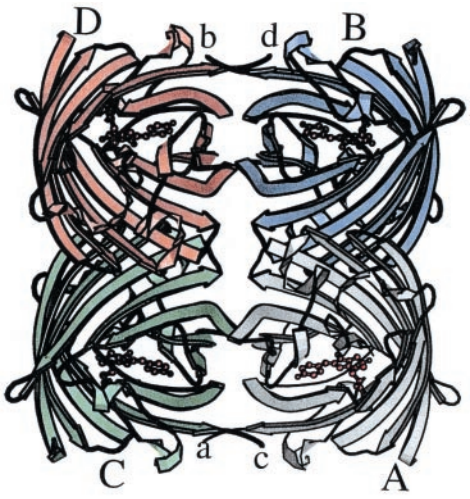

Fig. 2. Ribbon diagram of the DsRed tetramer, produced by MOLSCRIPT (28). Monomers are labeled with uppercase A–D, and the carboxy termini are labeled with lowercase a–d. The amino termini are obscured in this view. Note the antenna-like array of the chromophores, antiparallel in pairs.

tially exposed to solvent, the intimate association of Leu-225 with another protomer in the tetramer will likely result in nonfunctional carboxyl-terminal fusion constructions with DsRed. Much of the AC interface involves the bulge region of the fold (which contacts the chromophore), suggesting that tetramer formation may be important for correct folding and/or proper establishment of the chromophore environment. In an unusual pairwise interaction, His-A162 is involved in a stacking interaction with His-C162 of an adjacent molecule while simultaneously maintaining a salt bridge or hydrogen bond with Glu-C176, forming what appears to be an important part of the AC interface.

The Chromophore Environment. The DsRed chromophore, as predicted by sequence comparisons (4), is formed from a tripeptide located at the center of the coaxial helix. The chromophore, represented in stereo in the experimental electron density map in Fig. 3*A*, is formed by the autocatalytic cyclization and dehydrogenation of the -Gln-Tyr-Gly- (residues 66–68) tripeptide. The environment surrounding the chromophore is an extremely polar cavity with a number of interesting features represented in stereo in Fig. 3*B* and schematically in Fig. 3*C*. Considering the hydrogen bond and salt bridge network, the chromophore environment is much more complicated in DsRed than in avGFP [compare figure 2c of Ormo *et al.* (7)]. There are more buried charges in DsRed than in avGFP, including three new lysine residues (residues 70, 83, and 163) and a glutamic acid residue (residue 148) that interact closely with the chromophore. These charges are in a striking arrangement of two perpendicular bands, with the positive band roughly parallel to the long axis of the chromophore (and the transition dipole moment) and the negative band perpendicular to this axis, bisecting the chromophore (Fig. 3*C*). Lys-83, not shown, is included in the positive band.

The phenolate oxygen of the chromophore forms a hydrogen bond with Ser-146 (equivalent to avGFP His-148) as well as with a nearby water molecule. Surprisingly, the phenolate oxygen also forms an apparent charge–charge interaction with a neighboring buried lysine residue (Lys-163). This interaction and the number of hydrogen bonds require that the phenolate oxygen be charged at all times.

The conserved Glu-215, equivalent to avGFP Glu-222, is found in a similar position relative to the overall fold of the molecule, but in DsRed it not only is closer to the chromophore, but also interacts with a water molecule (W* in Fig. 3 *B* and *C*; see discussion below) that is strategically positioned near Gln-66. Glu-215 also interacts with the positively charged side chain of Lys-70, instead of forming a hydrogen bond with the Ser-205 side chain as in avGFP. As pointed out by Matz *et al.* (4), Ser-205 is replaced with Leu-199 in DsRed, which is driven ≈2.5 Å into the chromophore environment by the local collapse of the main chain mentioned above (Fig. 1). Thus, Glu-215 must be charged at all times, and no reversible proton transfer to it is possible via a relay network like that described for wild-type avGFP by Brejc *et al.* and Palm *et al.* (22, 23). Gln-213 and Asn-42 both serve via hydrogen bonding to position the Gln-66 side chain, which protrudes from and in the plane of the chromophore. Mutagenesis results suggest that this positioning is probably important for red fluorescence, as discussed below. Arg-95 is found in a position nearly identical to that of its counterpart avGFP Arg-96, making close contact with the imidazolinone oxygen of the chromophore.

As a last note, the four chromophores in the tetramer form an antenna-like rectangular array of approximately 27 by 34 Å (see Fig. 2), suggesting that efficient energy transfer between centers is possible. This may be important in considering evidence that a large fraction, perhaps 50%, of the chromophores do not appear to mature beyond the green-emitting stage (10). Should hybrid tetramers form, nonradiative energy transfer from green-emitting to red-emitting centers should be essentially 100% efficient, which will complicate the analysis. Whether such energy transfer and/or incomplete maturation has an important biological role is interesting to consider. The electron density map shows no evidence for incomplete chromophore formation, so if incomplete chromophores are present in the crystal, these are rotationally disordered within the four subunits.

Interpretation of Prior Mutagenesis Studies. Random and directed mutagenesis of DsRed has been used to investigate influences of the protein environment on chromophore maturation and spectral characteristics (6). Several interesting mutants have been described that affect these properties, and the three-dimensional structure offers some insight into the basis for these changes. The mutation of Lys-70 to Met (K70M) inhibits the final maturation step, resulting in a green fluorescent protein with spectral characteristics very similar to those of avGFP. This is not surprising, as this residue lies "on top of" and in direct contact with the chromophore (Fig. 3 *B* and *C*) and is part of an intricate charge network in the chromophore cavity. Lys-70 interacts with the buried charges of Glu-215 and Glu-148 (via a water molecule) and must be charged. Replacement with neutral Met must cause significant changes in this network. Mutations of Asn-42 can be similarly understood, as Asn-42 is involved in positioning the Gln-66 side chain (Fig. 3 *B* and *C*), which becomes part of the chromophore. The N42D mutant is green, which suggests that the mutated side chain is charged. Either the charge inhibits the final maturation to the red-emitting form, or the positioning of the Gln-66 side chain is not optimal in this mutant for further oxidation.

The cases of mutation at Lys-83 and Ser-197 can be rationalized as well. The K83R and K83N mutations result in green fluorescence, and the K83M substitution results in a surprisingly large redshift of both absorption and emission maxima (6). Lys-83 originates from a loop that connects the axial helix to one of the β strands and is located in a buried polar pocket, surrounded by water molecules. This residue makes very few direct interactions with other parts of the protein. However, its location places the primary amine close to the Lys-70 side chain, which does contact the chromophore. Perturbations of the packing near Lys-70 caused by the increased size of the Arg side chain (or reduced size of the Asn side chain) may be responsible for inhibiting the maturation. Met, on the other hand, is roughly isosteric with Lys but differs in charge. Substitution of K83 with Met would alter the chromophore charge distribution and consequently change the absorption and emission behavior. Likewise, Ser-197 interacts directly (and indirectly

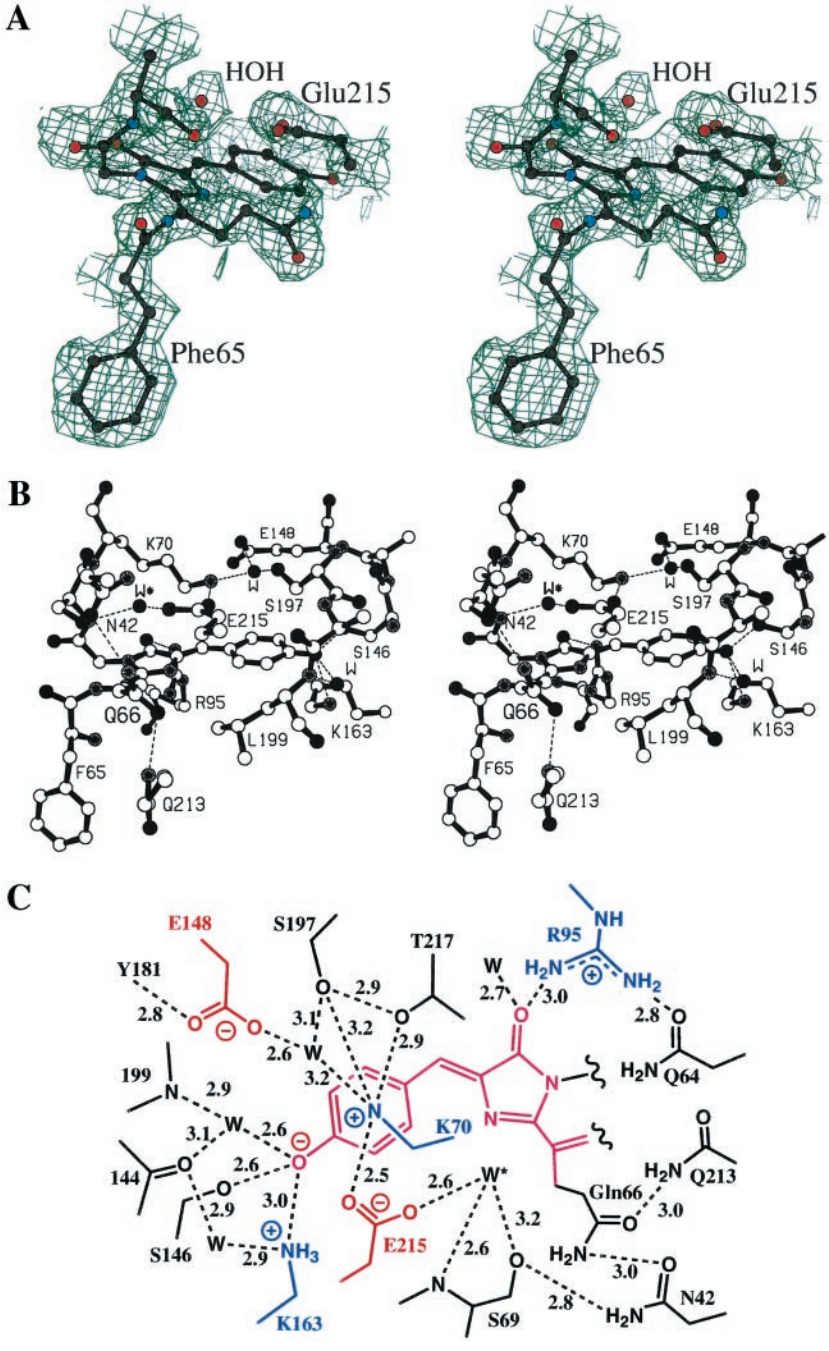

Fig. 3. (*A*) A portion of the experimental multiwavelength anomalous dispersion-phased electron density map at 2.0-Å resolution, contoured at 1.0 standard deviation. The refined model of the chromophore and some surrounding side chains are superimposed. (*B*) Ball-and-stick diagram of the DsRed chromophore and environment. Some important salt bridges and/or hydrogen bonds are indicated by dashed lines. (*C*) Schematic diagram of the chromophore environment showing salt bridges and/or hydrogen bonds (dashed), labeled with approximate lengths in angstroms. Charged residues in the vicinity of the chromophore are colored, and a proposed catalytic water molecule is indicated by W* (see text).

through a water molecule) with Lys-70, and the S197T replacement significantly affects final maturation (9). In each case, perturbation of the network involving Lys-70 seems to account for the observed changes in maturation behavior.

Structural Basis for Red Fluorescence. The observation that red fluorescence is preceded by a green-emitting intermediate suggests that there are several distinct steps in the overall reaction, as proposed by Matz *et al.* (4). To date, no generally accepted mechanism that defines the catalytic roles of specific protein side chains has been advanced for the maturation of any fluorescent protein, although it is generally agreed that the conserved amino acids avGFP Arg-96 and Glu-222 are very likely to be key players.

The data presented by Baird *et al.* and Gross *et al.* (6, 10), who suggested that chromophore formation in DsRed involves an oxidation step associated with Gln-66, led us to exclude the chromophore from the model in the early part of the refinement process. However, even in the original multiwavelength anomalous dispersion-phased electron density maps, it was clear that the avGFP chromophore could essentially completely account for the observed electron density (Fig. 3*A*). It was therefore obvious from early in the structural study that no new covalent bonds from other side chains to the chromophore had formed and that additional chemical steps leading to red fluorescence had to be rather subtle.

The geometry associated with the α carbon of Gln-66 was not restrained during refinement, and all four of the chromophores clearly adopted a planar geometry that is consistent with sp^2 hybridization of this center. The β-carbon and main-chain nitrogen of Gln-66 and the carbonyl carbon of Phe-65 are coplanar with the rest of the chromophore (Scheme 1 and Fig. 3 *A* and *B*). On the

other hand, despite its apparent conjugation with the rest of the chromophore, the C═O bond of Phe-65 is almost perpendicular to the plane of the chromophore. This was predicted by Gross *et al.* (10) on the basis of theoretical calculations, without knowledge of the structural results. The importance of this unexpected observation remains unclear, but the convergence of the theoretical calculations and the structural studies is remarkable.

Two points are clear from a comparison of the chromophores and their environments in DsRed and avGFP. First, the geometries of the α carbons of Gln-66 vs. Thr/Ser-65 are clearly different in the two instances, consistent with sp^2 hybridization in DsRed and sp^3 hybridization in avGFP. Second, the positioning of the conserved glutamate (Glu-215 vs. avGFP Glu-222) differs substantially relative to the chromophore. In the independent subunits of DsRed, Glu-215 is closer to the chromophore and is hydrogen bonded to a strategically located water molecule (W* in Fig. 3 *B* and *C*) that sits "above" the heterocycle close to the N—Cα bond of Gln-66, which becomes oxidized. W* may be a product of the final oxidation reaction. We suggest that the proper positioning of the Gln-66 and Glu-215 side chains is critical for red fluorescence. Furthermore, we suggest that Glu-215 plays more than one role in the maturation chemistry of DsRed, first in the formation of the green intermediate (in some unspecified role that is probably common to all FPs), and that the stereochemical environment of Glu-215 is crucial for the formation of both the green- and red-emitting species.

Matz *et al.* (4) suggested that avGFP is a "broken" version of an ancestral red fluorescent protein that is developmentally arrested at the stage of the green-emitting intermediate. The new structural results, revealing a more intricate and polar chromophore environment in DsRed, suggest otherwise. Red fluorescence appears to be a result of an extremely subtle interplay of a more highly evolved and optimized assemblage of active site residues than is the case for avGFP. Thus, it should not be a surprise if a very rapidly maturing version of DsRed cannot easily be found, and that most mutations in the vicinity of the chromophore are deleterious. In contrast, avGFP is surprisingly tolerant of substitutions in and near the chromophore (1, 8, 27). An interesting challenge would be to produce a monomeric version of DsRed; whether such a version already exists in nature or might be produced by mutagenesis of avGFP remains to be seen.

Note Added in Proof. We have reprocessed the SSRL data to 1.3 Å resolution and have continued to refine the atomic model. The crystallographic *R* factor is 0.161 for 191,847 unique observations and an overall completeness of 88% (20–1.3 Å resolution). Most of our previous conclusions are unchanged; however, it is now clear that the chromophore electron density represents a mixture of immature green and mature red species at roughly 50% occupancy each, in accord with the experimental results (10) discussed previously. Furthermore, the immature green species contains a cis peptide bond between residues Phe-65 and Gln-66 (not a peptide bond in the mature form, but trans in avGFP), and displays two predominant conformations of the side chain of Ser-69. In one presumably catalytic conformation, Oγ of Ser-69 is poised over the 66N-Cα bond in a position appropriate for proton abstraction, activated by Glu-215. A detailed mechanism for the final oxidation reaction leading to red fluorescence is proposed in Scheme 2. In this mechanism, the rate-limiting step in generating red fluorescence may be deprotonation of the α carbon of Gln-66 by Ser-69 Oγ (requiring prior cis–trans isomerization of the peptide bond), generating a reactive carbanion for attack by dioxygen via a superoxide radical anion intermediate. The oxidation reaction would then proceed via a hydroperoxide adduct and result in the release of hydrogen peroxide on completion.

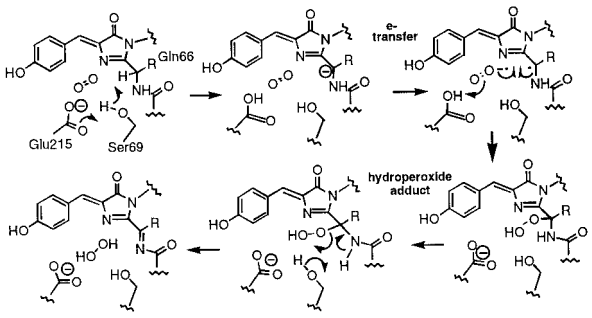

Scheme 2.

The carbanion and hydroperoxide intermediates proposed here have precedence in the luciferase literature. In the recently published crystal structure of aequorin, there is crystallographic evidence that the substrate coelenterazine is bound to as the hydroperoxide adduct (24), and a histidine side chain has been suggested as a base to initiate carbanion formation (24, 25). In beetle luciferases, it has been known for some time that the C4 proton of the imidazopyrazine substrate is removed during light generation, but only if the correct enantiomer is supplied.

Lys-70 would be important for maintaining Glu-215 as an anion, consistent with the failure of the K70M mutant to mature beyond the green emitting state. In avGFP, Ser-69 is replaced by Val-68; Glu-222 is positioned differently with respect to the chromophore, and the 64–65 peptide bond is trans, all of which would prevent further maturation.

This work was supported by a grant from the National Science Foundation (MCB 9728162 to S.J.R.), a National Institutes of Health postdoctoral fellowship (1F32GM19075-01 to R.M.W.), and a predoctoral traineeship (GM00759 to D.Y.). M.V.M. acknowledges partial support from CLONTECH.

1. Tsien, R. Y. (1998) *Annu. Rev. Biochem.* **67,** 509–544.
2. Remington, S. J. (2000) in *Bioluminescence and Chemiluminescence*, eds. Baldwin, T. O. & Sigler, M. M. (Academic, San Diego), Vol. 305, pp. 195–211.
3. Lukyanov, K. A., Fradkov, A. F., Gurskaya, N. G., Matz, M. V., Markelov, M. L., Zaraisky, A. G., Zhao, X., Fang, Y., Tan, W. & Lukyanov, S. A. (2000) *J. Biol. Chem.* **275,** 25879–25882.
4. Matz, M. V., Arkady, F. F., Labas, Y. A., Savitsky, A. P., Zaraisky, A. G., Markelov, M. L. & Lukyanov, S. A. (1999) *Nat. Biotechnol.* **17,** 969–973.
5. Dove, S., Takabayashi, M. & Hoegh-Guldberg, O. (1995) *Biol. Bull.* **189,** 288–297.
6. Baird, G. S., Zacharias, D. A. & Tsien, R. Y. (2000) *Proc. Natl. Acad. Sci. USA* **97,** 11984–11989.
7. Ormo, M., Cubitt, A. B., Kallio, K., Gross, L. A., Tsien, R. Y. & Remington, S. J. (1996) *Science* **273,** 1392–1395.
8. Wachter, R. M., Elsliger, M. A., Kallio, K., Hanson, G. T. & Remington, S. J. (1998) *Structure (London)* **6,** 1267–1277.
9. Terskikh, A., Fradkov, A. F., Ermakova, G., Zaraisky, A. G., Tan, P., Kajava, A. V., Zhao, X., Ding, L., Lukyanov, S. A., Matz, M. V., *et al.* (2000) *Science* **290,** 1585–1588.
10. Gross, L. A., Baird, G. S., Hoffman, R. C., Baldridge, K. K. & Tsien, R. Y. (2000) *Proc. Natl. Acad. Sci. USA* **97,** 11990–11995.
11. Van Duyne, G. D., Standaert, R. F., Karplus, P. A., Schreiber, S. L. & Clardy, J. (1993) *J. Mol. Biol.* **229,** 105–124.
12. Terwilliger, T. C. & Berendzen, J. (1999) *Acta Crystallogr. D* **55,** 849–861.
13. De LaFortelle, E. & Bricogne, G. (1997) *Methods Enzymol.* **276,** 472–494.
14. Abrahams, J. P. & Leslie, A. G. W. (1996) *Acta Crystallogr. D* **52,** 30–42.
15. Jones, T. A., Zou, J.-Y., Cowan, S. W. & Kjeldgaard, M. (1991) *Acta Crystallogr. A* **47,** 110.
16. Tronrud, D. E., Ten Eyck, L. F. & Matthews, B. W. (1987) *Acta Crystallogr. A* **43,** 489–503.
17. Tong, L. & Rossmann, M. G. (1997) *Methods Enzymol.*, **276,** 594–611.
18. Matthews, B. W. (1968) *J. Mol. Biol.* **33,** 491–497.
19. Yang, F., Moss, L. G. & Phillips, G. N. J. (1996) *Nat. Biotechnol.* **14,** 1246–1251.
20. Rossmann, M. G. & Argos, P. (1976) *J. Mol. Biol.* **105,** 75–95.
21. Lee, B. & Richards, F. M. (1971) *J. Mol. Biol.* **55,** 379–400.
22. Brejc, K., Sixma, T. K., Kitts, P. A., Kain, S. R., Tsien, R. Y., Ormo, M. & Remington, S. J. (1997) *Proc. Natl. Acad. Sci. USA* **94,** 2306–2311.
23. Palm, G. J., Zdanov, A., Gaitanaris, G. A., Stauber, R., Pavlakis, G. N. & Wlodawer, A. (1997) *Nat. Struct. Biol.* **4,** 361–365.
24. Head, J. F., Inouye, S., Teranishi, K. & Shimomura, O. (2000) *Nature (London)* **405,** 372–376.
25. Prendergast, F. G. (2000) *Nature (London)* **405,** 291–293.
26. Wood, K. V. (1995) *Photochem. Photobiol.* **62,** 662–673.
27. Wachter, R., King, B. A., Heim, R., Kallio, K., Tsien, R. Y., Boxer, S. G. & Remington, S. J. (1997) *Biochemistry* **36,** 9759–9765.
28. Kraulis, P. J. (1991) *J. Appl. Crystallogr.* **24,** 946–950.